Orthogonal tight-binding molecular-dynamics simulations of silicon clusters

B. K. Panda,[1] S. Mukherjee,[2] and S. N. Behera[1]
[1]*Institute of Physics, Sachivalaya Marg, Bhubaneswar-751005, India*
[2]*S. N. Bose National Centre for Basic Sciences, Block JD, Sector III, Salt Lake City, Calcutta 700091, India*
(Received 29 February 2000; revised manuscript received 10 August 2000; published 8 January 2001)

Orthogonal tight-binding molecular-dynamics methods are employed for describing small silicon clusters. Results obtained from the calculations of two different sets of tight-binding parameters are compared with one another and with those previously calculated using nonorthogonal tight-binding schemes and *ab initio* methods. Comparing the resulting cohesive energies and bond lengths, it is concluded that the orthogonal tight-binding matrix elements and repulsive potentials need to include the radial cutoff up to fourth-neighbor distance in diamond structure in order to reproduce *ab initio* results.

DOI: 10.1103/PhysRevB.63.045404 PACS number(s): 71.60.+z, 79.20.Mb, 73.30.+y

I. INTRODUCTION

It is hoped that in the future miniaturization of semiconductor microelectronics devices will be achieved using cluster-assembled semiconductors which are expected to have different properties than those of bulk semiconductors. Understanding the structure and properties of Si clusters is of great interest, as it is an important material in the microelectronics industry. Since there is no systematic experimental method to extract the equilibrium geometry of small Si clusters, a molecular-dynamics simulation has been used to optimize geometries of small Si clusters. The frequencies of the vibrational modes of these small clusters, measured recently using the Raman scattering technique, were compared with first-principles calculations in order to identify the stable geometries of clusters in an indirect manner.[1,2] Unfortunately, Raman spectroscopy measurements are available for Si clusters containing only up to seven atoms. Ion mobility measurements, on the other hand, are available to provide information about the shape of Si clusters containing many atoms.[3]

The molecular dynamics of small Si clusters require a full quantum-mechanical description due to the strong directional character of the covalent bonds. The first-principles Hartree-Fock method with correlation corrections was reasonably successful in describing small clusters.[5–8] Fournier *et al.*[9] used a linear combination of atomic orbitals with local-spin-density approximation (LCAO-LSDA) method to calculate structures of small Si clusters up to eight atoms. Since the local-density approximation (LDA) overbinds the atoms in a cluster, Fournier *et al.* included a generalized gradient approximation (GGA) method of Perdew and Wang[10] to estimate accurate cohesive energies and bond lengths in the LCAO scheme. Since it is a spin-polarized method, both singlet and triplet states of the clusters are reproduced.

The Car-Parrinello method within the local-density approximation (CP-LDA) method is the most ideal technique for studying semiconductor clusters.[11] In this method the density-functional theory is combined with the molecular-dynamics method to minimize both the electronic and ionic degrees of freedom. The cohesive energies and equilibrium structures of small Si clusters were successfully understood using this scheme.[12–16] Very recently, this method was employed to study the equilibrium structures of medium-sized Si clusters up to $N=18$ atoms.[17,18]

Although *ab initio* methods provide accurate electronic information, the one-electron picture of bonding in these methods requires vast computational time in order to optimize large clusters. The interatomic potential, on the other hand, is short ranged, and therefore is very efficient for the molecular-dynamics simulation studies. The Lennard-Jones two-body potential has been attractive for the study of noble gas[19] and simple metal clusters.[20] However, this model is unsuitable for understanding covalent systems with tetrahedral coordination. Classical potential models were applied to the study of small Si clusters.[21,22] Further, this model is not accurate in predicting the equilibrium structure of clusters, as it does not include electronic effects such as π bonding, which becomes increasingly important for small clusters. The other reason for the failure of this model is that clusters are rather weakly bound in classical model compared to quantum-mechanical calculations, due to the reduced number of neighbors included in the model.

Semiempirical tight-binding models in the two-center approximation[23] are popular for electronic structure calculations which are not possible in classical models. Unlike the CP-LDA method, where a large number of plane waves are taken into consideration to obtain the desired convergence of the results, tight-binding methods in Si require a minimal (s,p) basis set consisting of one s orbital and a set of three rotationally related p orbitals for each atom in order to describe bonding. Four bonding electrons are distributed among these orbitals. Occupation of the s and p orbitals by an electron requires on-site energies E_s and E_p. The two-center approximation of the tight-binding theory takes the pairwise coupling of the orbitals of nearby atoms to describe bonding. Orbitals of the neighboring atoms couple according to the interatomic distance and their rotational symmetry. The interaction between a pair of atoms in the nonorthogonal tight-binding scheme is described by four sets of Slater-Koster matrix elements[24] $V_{ss\sigma}$, $V_{sp\sigma}$, $V_{pp\sigma}$, and $V_{pp\pi}$, and the overlap integrals $S_{ss\sigma}$, $S_{sp\sigma}$, $S_{pp\sigma}$ and $S_{pp\pi}$ due to symmetry. In the orthogonal tight-binding scheme the orthogonalized atomic orbitals result in unity for the overlap integrals, which simplifies the calculations. The repulsive potential of atoms as they are brought together is assumed to

depend only upon the positions of the atoms, thus expressing it in a pairwise form. Since the electronic degrees of freedom are not explicitly included in the molecular-dynamics simulation, large time steps can be safely used. Moreover, this method works faster than the *ab initio* methods, as it minimizes only the atomic degrees of freedom.

Tománek and Schlüter used density-functional and empirical tight-binding schemes to calculate electronic structure of small Si clusters.[25] Laasonen and Nieminen[26] employed the Car-Parrinello method in the empirical orthogonal tight-binding scheme for calculating cohesive energies and geometries of small clusters upto $N=10$. In both methods the interparticle repulsive potential is obtained from the difference of the interparticle dependence of the energy of the Si dimer and the tight-binding energy. In order to obtain reasonable agreement with the *ab initio* values of cohesive energies, a coordination-dependent bond correction energy term is taken in these calculations. The matrix elements are terminated between first- and second-neighbor distances. The geometries of relatively large clusters in these methods do not agree with those predicted by accurate *ab initio* calculations.[8]

Nonorthogonal tight-binding molecular-dynamics techniques,[27–30] on the other hand, have been found to optimize geometries of small clusters in good agreement with the *ab initio* techniques.[8,9] The correction to the energy due to the bond counting term is not necessary in the binding energy and force calculations. The advantage of this method over an orthogonal scheme is that this method does not require any cutoff distance for the matrix elements and overlap integrals. The vibrational frequency analysis in small clusters has shown that the tight-binding scheme without nonorthogonality cannot reproduce the *ab initio* results.

In terms of computational cost, the semiempirical orthogonal tight-binding method is found to be the most efficient, as the inclusion of the nonorthogonality makes the calculation of energies and forces slower. The only important task in the orthogonal method is to make Slater-Koster matrix elements transferable by a suitable method. In an early approach, Harrison[23] and Chadi[31] used the $1/d^2$ dependence of tight-binding hopping matrix elements with a bond length d. Mercer and Chou[32] fitted tight-binding parameters to *ab initio* band structures based on a norm-conserving pseudopotential method, and found that a simple $1/d^2$ scaling is not correct for transferability. Since the inclusion of the second neighbor in the calculations gives incorrect results, Goodwin, Skinner, and Pettifor (GPS)[33] and Sawada[34] presented independent schemes where the tight-binding matrix elements and the pairwise repulsive potentials are smoothly terminated by attenuation functions between the first and second neighbors, so as to avoid discontinuity in the potential. Kohyama[35] showed that the method of Sawada is superior to that of GPS for describing the binding energies and equilibrium volumes of various coordinated structures in Si. Kwon *et al.*[36] overcame the shortcomings of the GPS model by fitting each matrix element in the GPS model, and produced bulk and defect properties of Si in good agreement with the *ab initio* methods and experiment. The pair repulsive potential is obtained in the embedded atom model.[37] Lenosky *et al.*[38] obtained the matrix elements and pair repulsive potential as cubic splines with a 5.24-Å fixed radial cutoff distance which is the fourth-neighbor distance in diamond structure. Using the force matching method,[39] the spline parameters have been fitted to simultaneously optimize agreement with *ab initio* force and energy data on clusters, liquids, and amorphous systems, as well as experimental elastic constants, phonon frequencies, and Grüneisen parameter values. The orthogonal tight-binding matrix elements and the pair repulsive potentials obtained by this method are claimed to be the best among all previous works.

The orthogonal tight-binding model of Sawada and Kohyama have been combined with the fractional bond model of Luo *et al.*[40] in order to optimize geometries of Si clusters up to $N=10$. The cohesive energies and equilibrium geometries obtained in this method agree very well with *ab initio* results up to $N=7$ clusters. The results for clusters ($N>7$) do not compare well with the *ab initio* results. We therefore feel it necessary to test the validity of the other orthogonal models by Kwon *et al.* and Lenosky *et al.* for optimization of cluster geometries upto $N=19$ before entirely rejecting the semiempirical orthogonal methods for small Si cluster simulations. The second motivation is to verify the conclusion of the nonorthogonal tight-binding schemes[27,28] about the incorrectness of the orthogonal tight-binding schemes in estimating the vibrational frequency of the dimer. We are encouraged to follow these two orthogonal tight-binding models, as these models have already been successful in understanding small Si clusters up to $N=5$.

A recent experimental determination of the static polarizabilities for a Si_N ($N\geqslant 9$) cluster in beam deflection under an electric field[41] indicates pronounced oscillations with the cluster size. For large clusters ($60<N<120$) the polarizabilities reach values below the bulk limit. The orthogonal tight-binding calculations using the Harrison scaling scheme by Rantala *et al.*[42] resulted in large polarizabilities compared to the experimental data. The calculated polarizabilities for small clusters ($2\leqslant N\leqslant 10$) in the pseudopotential method of Vasiliev *et al.*[15] are higher than the bulk limit, and tend to reach above the bulk limit for large clusters. Since our tight-binding scheme is superior to that of Rantala *et al.*, it is worth applying our method for estimating polarizabilities for Si clusters.

The paper is organized as follows. The method for calculating the equilibrium geometries and static polarizabilities for Si clusters will be discussed in Sec. II. The calculated electronic and chemical properties will be discussed in Sec. III, and we give future directions in Sec. IV.

II. METHOD OF CALCULATIONS

A. Tight-binding molecular dynamics

The tight-binding energy governing atomic motions is given by

$$E=\sum_{i=1}^{N}\frac{\mathbf{p}_i^2}{2M}+2\sum_{n}^{occ.}\langle|\Psi_n|H|\Psi_n\rangle+E_{rep}, \qquad (1)$$

where $\Psi_n(\mathbf{r})$ is the electronic wavefunction for nth level of the eigenstate. The first term is the kinetic energy of the atoms with mass M. The second term is the electronic energy obtained by summing the lowest eigenvalues of the tight-binding Hamiltonian H. Two electrons are assigned to each eigenstate to account for the spin. The third term E_{rep} represents the combined repulsive energy and the energy required for correcting the double counting of the electron-electron interaction of the second term. The $\Psi_n(\mathbf{r})$ of a collection of atoms as a linear combination of orthogonalized basis functions $\phi_\nu(\mathbf{r})$, in the minimum basis set ($\nu = s, p_x, p_y, p_z$), is expanded as

$$\Psi_n(\mathbf{r}) = \sum_{\nu i} C^n_{\nu i} \phi_\nu(\mathbf{r} - \mathbf{R}_i), \tag{2}$$

where $\mathbf{R}_i$ denotes the position of the ith atom. The eigenvalues are obtained from the Schrödinger equation as

$$\sum_{\nu\mu, ij} [H_{\nu\mu}(\mathbf{r}_{ij}) - \delta_{\mu\nu}\delta_{ij}E_n] C^n_{\nu i} = 0, \tag{3}$$

where $\mathbf{r}_{ij} = \mathbf{R}_i - \mathbf{R}_j$. The tight-binding matrix elements are obtained from the two-center hopping integral:

$$H_{\nu\mu}(\mathbf{r}_{ij}) = \int \phi^*_\nu(\mathbf{r} - \mathbf{R}_i) H \phi_\mu(\mathbf{r} - \mathbf{R}_j) d^3r. \tag{4}$$

Following the Slater-Koster method,[24] the matrix elements in Eq. (3) are expressed as

$$\begin{aligned} H_{ss} &= V_{ss\sigma}(\mathbf{r}_{ij}) \\ H_{sx} &= -H_{xs} = l_{ij} V_{sp\sigma}(\mathbf{r}_{ij}) \\ H_{xx} &= l^2_{ij} V_{pp\sigma}(\mathbf{r}_{ij}) + (1 - l^2_{ij}) V_{pp\pi}(\mathbf{r}_{ij}) \\ H_{xy} &= H_{yx} = l_{ij} m_{ij} V_{pp\sigma}(\mathbf{r}_{ij}) - l_{ij} m_{ij} V_{pp\pi}(\mathbf{r}_{ij}), \end{aligned} \tag{5}$$

where l_{ij} and m_{ij} are the directional cosines.

The transferable matrix elements $V_{ss\sigma}(\mathbf{r})$, $V_{sp\sigma}(\mathbf{r})$, $V_{pp\sigma}(\mathbf{r})$, and $V_{pp\pi}(\mathbf{r})$, as given by the models of Kwon *et al.*[36] and Lenosky *et al.*,[38] are shown in Fig. 1. It is quite clear that potentials in the model by Kwon *et al.* decay monotonically, whereas those in the model of Lenosky *et al.* are highly nonlinear in nature. As discussed earlier, the matrix elements in the model of Kwon *et al.* are seen to go smoothly to zero between first and second neighbors, whereas those for the model of Lenosky *et al.* are extended to fall smoothly between the third and fourth neighbors. Lenosky *et al.* pointed out that a long cutoff of 5.24 Å is needed in order to place the clathrate structure higher in energy than the diamond structure, whereas the small cutoff in the potentials of Kwon *et al.* shows a clathrate structure lower in energy than the diamond structure. The lower limit of the extent of the potentials in the model of Lenosky *et al.* is fixed at 1.5 Å as the potential is very strong below this limit. In reality the potentials should saturate, and approach a constant value at short distances. However, such adjustments lead to unphysically small values of the Grüneisen parameters. Unlike the model of Kwon *et al.* $V_{ss\sigma}(\mathbf{r})$ in the model

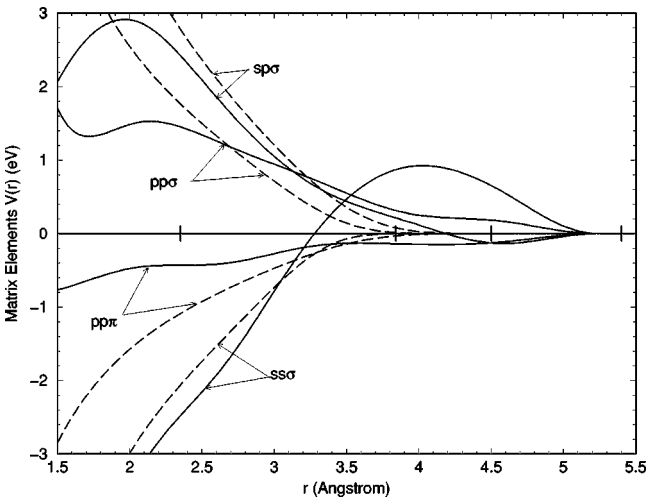

FIG. 1. Matrix elements $V_{ss\sigma}(r)$, $V_{sp\sigma}(r)$, $V_{pp\sigma}(r)$, and $V_{pp\pi}(r)$ in the orthogonal tight-binding models of Refs. 38 (solid line) and 36 (long-dashed line). The short vertical lines in the zero y axis correspond to the first four neighbor shells in the diamond structure.

of Lenosky *et al.* changes sign between first and second neighbors, and shows a fairly large and positive hump at 4 Å. Similarly $V_{sp\sigma}$ in the model of Lenosky *et al.* changes sign between second and third neighbors and has a large hump at 2 Å. Although $V_{pp\sigma}(\mathbf{r})$ and $V_{pp\pi}(\mathbf{r})$ in the model of Lenosky *et al.* preserve their sign as in the model of Kwon *et al.*, there are many structures present in these data. The electronic energy in the model of Kwon *et al.* is found to be larger than that in the model of Lenosky *et al.*

The repulsive potential E_{rep} in the method of Kwon *et al.*[36] is given by

$$E_{rep} = \sum_i f\left[\sum_j \Phi(\mathbf{r}_{ij})\right], \tag{6}$$

where in general the function $f(x)$ in the embedded-atom approach is expressed as

$$f(x) = C_1 x + C_2 x^2 + C_3 x^3 + C_4 x^4. \tag{7}$$

In the model of Lenosky *et al.* the cubic splines are taken without any functional form. Therefore, it corresponds to the case $C_1 = 1$, $C_2 = C_3 = C_4 = 0$. The interparticle pair repulsive potential is shown in Fig. 2. We find that the pair potential appears to grow monotonically as the interparticle separation decreases. The potential used by Kwon *et al.* is more strongly repulsive in the short interparticle separation compared to that of Lenosky *et al.* and it also decays quite fast in the first-neighbor region. The potential of Lenosky *et al.* goes smoothly to zero between third and fourth neighbors, while that of Kwon *et al.* falls to zero between first and second neighbors. The repulsive energy E_{rep}, calculated using the embedded energy functional $f(x)$ in the model of Kwon *et al.*, is found to be stronger than that of Lenosky *et al.* However, E_{rep} in both models is found to be insensitive to to details of the cluster geometry.

The force acting on the ith ion is expressed as

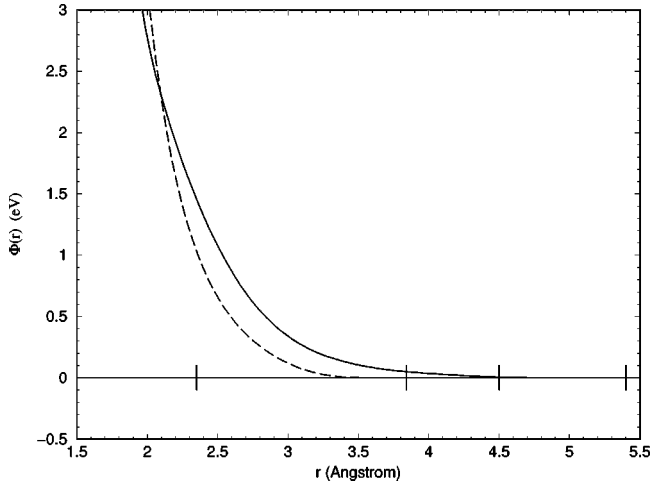

FIG. 2. Repulsive pair potential in the orthogonal tight binding models of Refs. 38 (solid line) and 36 (long-dashed line). The short vertical lines in the zero *y* axis correspond to the first four neighbor shells in the diamond structure.

$$\mathbf{F}_i = -2\sum_n \langle \Psi_n | \frac{\partial H}{\partial \mathbf{R}_i} | \Psi_n \rangle - \frac{\partial E_{rep}}{\partial \mathbf{R}_i}. \tag{8}$$

The first term is the Hellman-Feynman contribution to the total force evaluated from the derivatives of the matrix elements of the tight-binding Hamiltonian *H*. The second term is the short-ranged repulsive force.

Following the classical description of Newton's law the atomic positions are determined by

$$M\frac{d^2\mathbf{R}_i}{dt^2} = \mathbf{F}_i, \tag{9}$$

where *M* is the atomic mass. The solution of Eq. (9), in the velocity Verlet molecular dynamics method[43] for updating atomic coordinates, is given by

$$\mathbf{R}_i(t+\delta t) = \mathbf{R}_i(t) + \mathbf{v}_i(t)\,\delta t + \frac{1}{2M}\mathbf{F}_i(t)(\delta t)^2, \tag{10}$$

where the velocity $\mathbf{v}_i$ of *i*th atom at $t+\delta t$ is calculated from $\mathbf{F}_i$ at *t* and $t+\delta t$ as

$$\mathbf{v}_i(t+\delta t) = \mathbf{v}_i(t) + \frac{1}{2M}[\mathbf{F}_i(t) + \mathbf{F}_i(t+\delta t)]\,\delta t. \tag{11}$$

For molecular-dynamics studies the simulated annealing scheme is a generalized minimization procedure for finding a global minimum. There are various schemes to carry out simulated annealing studies.[26,44,45] In our case we have used the simple quenching and annealing method as prescribed by Ordejón *et al.*[28] In this method the atomic velocities are set to zero whenever the intrinsic temperature exceeds the given temperature. This procedure like all other simulated annealing methods does not lead to the global minimization, but resulted in a metastable state. For this purpose we have chosen different plausible configurations for the initial atomic positions $\mathbf{R}_i$. For large clusters the initial geometries are taken from the *ab initio* works.[8,9]

B. Calculation of static polarizability

The equilibrium geometries of small Si clusters are then used to calculate their static polarizabilities and dipole moments. We have used the perturbation method to evaluate the electronic energies $E(\mathbf{F})$ in the presence of an electric field of strength $\mathbf{F}$. The tensor components of the static polarizability ($\alpha_{kk'}$) are calculated as[15,46]

$$\alpha_{kk'} = -\frac{\partial^2 E(\mathbf{F})}{\partial F_k \partial F_{k'}}, \tag{12}$$

where $k,k' = \{x,y,z\}$. The *k*th component of the dipole moment p_k is calculated from the total energy as

$$p_k = \frac{\partial E(\mathbf{F})}{\partial F_k}. \tag{13}$$

In second-order perturbation theory,[47] the total energy at the field strength $\mathbf{F}$ is given by

$$E(\mathbf{F}) = E_0 + e\sum_n^{all} \langle \Psi_n | \mathbf{F}\cdot\mathbf{r} | \Psi_n \rangle + 2e^2 \sum_n^{occ.} \sum_m^{unocc.} \frac{|\langle \Psi_n | \mathbf{F}\cdot\mathbf{r} | \Psi_m \rangle|^2}{E_n - E_m}, \tag{14}$$

where *e* is the electronic charge and E_0 is the ground-state electronic energy at $\mathbf{F}=0$. Using Eqs. (12), (13), and (14) the dipole moment per atom in the direction *k* is derived as

$$p_k = \frac{e}{N}\sum_n^{all} \langle \Psi_n | r_k | \Psi_n \rangle. \tag{15}$$

Similarly the polarizability component $\alpha_{kk'}$ per atom is found as

$$\alpha_{kk'} = -\frac{4e^2}{N}\sum_n^{occ.}\sum_m^{unocc.} \frac{\langle \Psi_n | r_k | \Psi_m \rangle \langle \Psi_m | r_{k'} | \Psi_n \rangle}{E_n - E_m}. \tag{16}$$

Using the atomic wave functions [Eq. (2)] in Eq. (15), the dipole moment per atom is derived as

$$p_k = \frac{e}{N}\sum_n^{all}\sum_{\nu i}\sum_{\mu j} C^n_{\nu i} {}^* C^n_{\mu j} \Delta^k_{\nu i,\mu j}, \tag{17}$$

where $\Delta^k_{\nu i,\mu j}$ may be defined as

$$\Delta^k_{\nu i,\mu j} = \int \Phi^*_\nu(\mathbf{r}-\mathbf{R}_i) r_k \Phi_\mu(\mathbf{r}-\mathbf{R}_j) d^3r. \tag{18}$$

Similarly the components of the polarizability are derived as

$$\alpha_{kk'} = -\frac{4e^2}{N} \sum_{n}^{occ.} \sum_{m}^{unocc.} \sum_{\nu i} \sum_{\mu j} \sum_{\xi i'} \sum_{\zeta j'} C^n_{\nu i} {}^* C^m_{\mu j} C^m_{\xi i'} {}^* C^n_{\zeta j'} \times \Delta^{k}_{\nu i,\mu j} \Delta^{k'}_{\xi i',\zeta j'} / (E_n - E_m). \quad (19)$$

It is worth pointing out that Rantala *et al.*[42] in their calculations did not include position vectors in the atomic wave functions. In reality we have no access to the atomic obitals in the orthogonal tight-binding model which are needed to compute Eqs. (17) and (19). In the present work we have taken the *s* and *p* wave functions from a separate free atom method. The exact method of calculation for the dipole moment and polarizability in the orthogonal tight-binding method should be based on the diagonal ansatz where the position operator is assumed to be diagonal in the tight binding representation, with elements reflecting the coordinates of the atoms. In this approach the dipole moment is derived as

$$p_k = \frac{e}{N} \sum_{n}^{all} \sum_{\nu k} C^n_{\nu k} {}^* C^n_{\nu k} R_k . \quad (20)$$

The polarizability per atom is found as

$$\alpha_{kk'} = -\frac{4e^2}{N} \sum_{n}^{occ.} \sum_{m}^{unocc.} \sum_{\nu k} \sum_{\mu k'} C^n_{\nu k} {}^* C^m_{\nu k} C^m_{\mu k'} {}^* C^n_{\mu k'} \times R_k R_{k'} / (E_n - E_m). \quad (21)$$

The average polarizability which is usually compared with the experiment is calculated from the diagonal components as

$$\langle \alpha \rangle = \tfrac{1}{3} (\alpha_{xx} + \alpha_{yy} + \alpha_{zz}). \quad (22)$$

III. RESULTS AND DISCUSSIONS

The TBMD code of Colombo[48] is suitably modified for carrying out calculations for small clusters. We have compared results obtained in the models of orthogonal tight-binding schemes with the latest nonorthogonal scheme of Menon and Subbaswamy[30] and gradient corrected LCAO-LSDA results of Fournier *et al.*[9] Hobday *et al.*[49] presented structures of small Si clusters up to $N=14$ atoms using a genetic algorithm. However, geometries in this calculation are not accurate compared to *ab initio* results for large clusters and the cohesive energies and bond lengths are not reported for comparison. We have also not considered clusters beyond $N=19$ since, starting from Si_{19}, there is a known discrepancy between the CP-LDA theory[18] and mobility measurements[3,4] about the transition of the prolate structures to compact cagelike structures.

The most important contribution of the model of Lenosky *et al.* over other tight-binding schemes is to assign zero energy to the isolated atom as in the *ab initio* methods. The energies of the isolated atom in the orthogonal tight binding scheme of Kwon *et al.*[36] and the nonorthogonal scheme of Menon and Subbaswamy[30] are -0.63 and -1 eV, respectively. Lenosky *et al.* attributed equal and opposite value of 5.670225 eV to the on-site matrix elements E_s and E_p in order to assign zero value to the cohesive energy of the isolated atom. The high magnitude $E_s - E_p = -11.340450$ eV compared to the other tight-binding schemes is due to the large cutoff distance taken for fitting matrix elements. The time step δt in this calculation is taken to be 1 fsec, and the total time for molecular dynamics simulation is taken to be 15 psec.

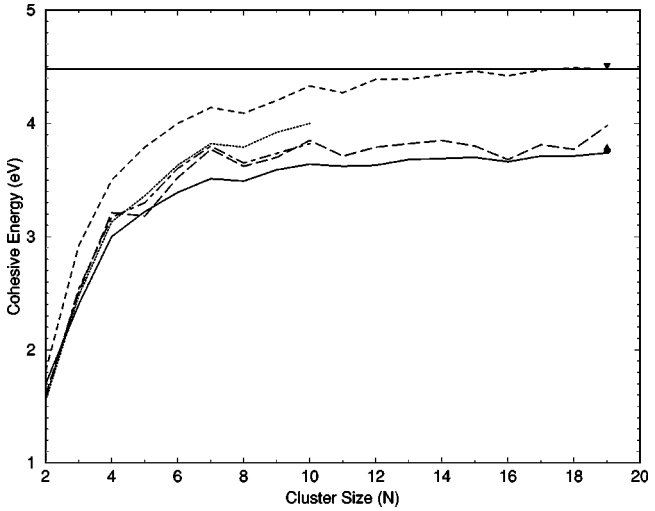

FIG. 3. Cohesive energies of Si clusters in the orthogonal tight binding models of Ref. 38 (solid line), the orthogonal tight binding method of Ref. 36 (long-dashed line), the CP-LDA (Refs. 18 and 17) (dashed line), the nonorthogonal tight-binding method of Ref. 30 (dotted line), and the gradient-corrected LCAO-LSDA (Ref. 9) (dot-dashed line) method. The cohesive energies for the cagelike structure of the Si_{19} cluster in the methods of Lenosky *et al.*, Kwon *et al.*, and the CP-LDA method are represented by the filled circle, the filled triangle, and the inverted filled triangle, respectively.

The cohesive energies for Si_N clusters upto $N=19$ calculated using different methods are reported in Fig. 3. The cohesive energy in the CP-LDA method[18,17] approaches that of the bulk semiconductor for medium-sized clusters. Ramakrishna and Bahel[14] pointed out that the higher cohesive energy results from the overbinding of atoms due to the LDA scheme, which can be rectified by a GGA method. The orthogonal tight binding scheme of Lenosky *et al.* predicted low cohesive energies for all clusters. This is expected on the physical grounds that the surface to volume ratio in small and medium sized clusters is rather large; as a consequence; the cluster cohesive energies will necessarily be smaller than the respective bulk values. On the other hand, the cohesive energies calculated in the orthogonal tight-bind model of Kwon *et al.*[36] agree with those in the Hartree-Fock calculations for Si clusters up to $N=10$. The nonorthogonal tight-binding scheme of Menon and Subbaswamy[30] found cohesive energies similar to that of the Hartree-Fock[7] results by a constant shift of 1.1 eV. This could be assigned to the zero-point energy of the isolated atom which is 1 eV.[38] For the Si_{19} cluster we have calculated cohesive energies for both the prolate and cagelike structures given by Ho *et al.*[17] The results are shown in Table I. We find that the orthogonal tight-binding scheme of Lenosky *et al.* predicted a cagelike structure for Si_{19}, which agrees with the CP-LDA method. The

TABLE I. Cohesive energy per atom of Si_{19} cluster in cagelike and prolate structures. The results are obtained using the orthogonal tight binding models of Refs. 38 (Orthogonal 1) and 36 (Orthogonal 2), and the Car-Parrinello local-density approximation (CP-LDA) (Ref. 17).

N	Orthogonal 1 (eV/N)	Orthogonal 2 (eV/N)	CP-LDA (eV/N)
19a	3.76	3.79	4.503
19b	3.74	3.98	4.481

model of Kwon *et al.*, on the other hand, found the prolate structure to be more stable than the cagelike structure.

The bond lengths for Si clusters up to $N=18$ are reported in Table II. The experimental cohesive energy for the Si dimer is 1.65 eV/atom.[50] Both orthogonal and nonorthogonal methods show similar cohesive energies and agree with the experiment. On the other hand, the cohesive energy calculated in the gradient corrected LCAO-LSDA method is very high. This method predicts that the spin-triplet state has a higher cohesive energy than the spin-singlet state. In the present spin-unpolarized calculation, the spin-singlet state of the dimer has a lower cohesive energy. It is worth mentioning that the orthogonal tight-binding schemes of Tománek and Schlüter,[25] Laasonen and Nieminen,[26] and Mercer and Chou[32] found the cohesive energies to be 1.54, 1.5, and 1.6 eV/atom, respectively, which are similar to our reported values. In spite of the dimer being in the singlet state and having lower cohesive energy in the model of Lenosky *et al.*, the bond length calculated in this method is exactly same as in the gradient corrected LCAO-LSDA method. The model of Kwon *et al.* gave longer bond lengths due to lower cohesive energy as calculated in this method. The earlier Hartree-Fock calculations of Raghavachari and Logovinsky[5] for the singlet state of the dimer resulted a cohesive energy of 1.58 eV/atom, a bond length to be 2.23 Å, which are similar to our values reported here. The experimentally determined bond length[52] of the Si dimer is is 2.24 Å.

The configurations of the Si clusters for $N=3-19$ are shown in Fig. 4. The gradient corrected LCAO-LSDA calculation showed that Si_3 is an equilateral triangle with sides of length 2.27 Å. Its ground state is a spin triplet with D_{3h} symmetry. On the other hand, the orthogonal tight-binding schemes predict the structure to be an isoceles triangle with C_{2v} symmetry. The D_{3h} symmetry is associated with the spin-triplet state, whereas the C_{2v} symmetry is a Jahn-Teller distortion of the D_{3h} symmetry. The singlet state of this cluster in the LCAO-LSDA method was been predicted to have a larger apex angle than that found in our calculations. On the other hand, the nonorthogonal tight-binding scheme[28] showed that the structure of the Si_3 cluster is an isoceles triangle with bond length and apex angle similar to our results. Our results also agree with the earlier singlet state calculations of the three atom cluster in the *ab initio* Hartree-Fock method.[5] The experimental value of the cohesive energy[51] for this cluster is 2.51 eV/atom, which matches with the results of Kwon *et al.*, and is slightly higher than that of Lenosky *et al.* We therefore believe that our calculation for both the dimer and trimer lie between the singlet and triplet states. The bond lengths calculated in the model of Kwon *et al.* are longer compared to other methods.

The gradient corrected LCAO-LSDA calculation predicted the four-atom cluster to be a rhombus in the singlet state with four bond lengths at 2.32 Å and the shortest interatomic bridge distance 2.40 Å. Recent Raman spectroscopy measurements[2,1] support this structure. However, our calculation agrees with the triplet state of the LCAO-LSDA calculation which is also a rhombus with lower cohesive energy. A nonorthogonal scheme[28] also calculated the geometry of this cluster in a triplet state. The model by Lenosky *et al.* is superior to the model of Kwon *et al.* for predicting the cohesive energy and bond lengths for this cluster. The geometry suggests that the main bonding in this cluster is primarily governed by π bonds.

As predicted by the gradient corrected LCAO-LSDA calculations, the five-atom cluster is a singlet state with trigonal bipyramid structure. Our calculations also show similar geometry. The nonorthogonal tight-binding scheme also predicted results comparable to the LCAO-LSDA model. However, the model of Lenosky *et al.* found cohesive energy and bond lengths in excellent agreement with LCAO-LSDA calculations better than those of Kwon *et al.*

The six-atom cluster in the *ab initio* LCAO-LSDA method is found to have both face-capped trigonal bipyramid and edge-capped trigonal bipyramid structures with identical binding energies. These two structures are in the singlet state with C_{2v} symmetry. It is hard to distinguish these two structures theoretically. Experimental Raman spectroscopy data[2] suggest the tetragonal bipyramid structure with D_{4h} symmetry which is not a stable structure in the gradient corrected LCAO-LSDA method. We have reported a face-capped trigonal bipyramid structure which is in excellent agreement with the LCAO-LSDA method. We have not compared our results with the nonorthogonal tight-binding scheme, as it has reported bond lengths only for the edge-capped trigonal bipyramid structure.[52]

The minimum energy of the seven atom Si cluster is found to be a pentagonal bipyramid with D_{5h} symmetry. The cohesive energy calculated by the model of Lenosky *et al.* is in good agreement with the gradient corrected LCAO-LSDA method. The two axial atoms are highly compressed in the gradient-corrected LCAO-LSDA method compared to the Si_6 cluster. The distances between two axial atoms in the models of Lenosky *et al.* and Kwon *et al.* are similar to nonorthogonal calculations[28] and previous orthogonal calculations.[25,26] Raman spectroscopy measurements support the gradient-corrected LCAO-LSDA results.

The Si_8 cluster is a distorted bicapped octahedron with C_{2h} symmetry. We find both binding energy and bond lengths to be in good agreement with gradient-corrected LCAO-LSDA, nonorthogonal, and CP-LDA methods.

For the Si_9 cluster we find that the tricapped octahedron structure predicted by the previous *ab initio* Hartree-Fock,[8] nonorthogonal,[28] and orthogonal tight-binding[25,26] schemes is not the lowest minimum structure. Both CP-LDA and full-potential linear-muffin-tin-orbital (FP-LMTO) methods[53] found it to be a bicapped pentagonal structure with C_{2v} sym-

TABLE II. Equilibrium geometries for silicon clusters for $N=2-18$. The atoms are numbered as in Fig. 4. The references to different models are the same as in Table I.

N	Structure	Bond	Orthogonal 1 (Å)	Orthogonal 2 (Å)	Nonorthogonal (Å)	*Ab initio* (Å)
2		1-2	2.28	2.45	2.24	2.28
3	C_{2v}	1-2	2.28	2.42	2.24	2.18
		1-3	2.73	2.89	2.80	2.84
		θ	73.7°	73.3°	77.4°	81.3°
4	D_{2h}	1-2	2.57	2.57	2.52	2.53
		1-3	2.33	2.49	2.34	2.27
		3-4	3.90	4.24	3.94	3.78
5	D_{3h}	1-2	3.20	3.52	3.26	3.05
		1-3	2.36	2.49	2.34	2.30
		3-4	2.94	2.74	2.78	2.98
6	C_{2v}	1-2	3.00	2.74		2.68
		1-3	2.38	2.54		2.35
		1-5	2.44	2.59		2.39
		3-5	2.52	2.64		2.71
		5-6	2.42	2.44		2.49
7	D_{5h}	1-2	2.88	2.78	2.80	2.51
		3-4	2.38	2.56	2.48	2.49
		1-3	2.51	2.58	2.47	2.46
		3-5	3.86	4.13		4.03
8	C_{2h}	1-2	2.67	2.64		2.48
		1-4	3.22	3.40		2.80
		1-5	2.38	2.53		2.40
		1-7	2.30	2.43		2.27
		2-3	3.03	2.90		2.88
		2-5	2.47	2.63		2.77
		2-6	3.89	3.91		4.00
		4-6	2.67	2.64	2.60	2.52
		5-6	3.03	2.90	4.00	3.14
		2-4	2.38	2.54	2.41	2.23
		4-8	2.30	2.43	2.52	2.53
9	C_{2v}	1-4	2.46	2.55		2.43
		2-3	2.88	2.72		2.53
		2-8	2.36	2.50		2.36
		6-7	3.18	3.06		2.85
		1-6	2.38	2.54		2.38
		6-8	2.34	2.57		2.37
		4-5	3.70	4.04		3.95
10	C_{3v}	1-2	3.06	2.89	2.91	2.75
		1-9	2.45	2.63	2.61	2.55
		5-9	2.47	2.60	2.56	2.54
		1-10	2.35	2.53	2.43	2.35
		1-3	2.38	2.52	2.49	3.45
		3-9	2.47	2.57	2.55	2.54

TABLE II. (*Continued*).

N	Structure	Bond	Orthogonal 1 (Å)	Orthogonal 2 (Å)	Nonorthogonal (Å)	*Ab initio* (Å)
11	C_{3v}	1-3	2.37	2.57		
		1-5	2.32	2.54		
		3-4	2.94	2.94		
		3-5	2.61	2.61		
		3-6	2.54	2.65		
		3-8	2.39	2.51		
		3-9	3.94	3.93		
		5-9	2.78	2.63		
		6-7	2.50	2.66		
		6-8	2.48	2.54		
		9-10	2.86	2.86		
12	C_{2v}	1-2	2.35	2.47		
		1-3	3.11	2.65		
		2-3	2.41	2.60		
		2-5	3.00	2.74		
		2-6	2.32	2.53		
		2-11	2.73	2.62		
		3-11	2.53	2.58		
		4-10	2.73	2.62		
		5-8	2.38	2.57		
		5-12	3.47	3.82		
		6-12	3.83	2.74		
		8-9	3.26	3.30		
		8-10	3.95	3.96		
		8-11	2.80	2.66		
		8-12	2.38	2.50		
		10-12	2.55	2.57		
13	C_{1h}	1-2	2.35	2.51		
		2-4	3.00	2.68		
		2-6	3.21	2.96		
		5-8	2.51	2.56		
		5-9	2.39	2.62		
		6-7	2.53	2.56		
		6-11	2.38	2.64		
		7-11	2.40	2.53		
		9-10	2.64	2.74		
		10-13	2.40	2.53		
14	C_{1h}	1-2	2.41	2.56		
		1-3	2.37	2.58		
		1-5	2.67	2.55		
		2-3	2.80	2.64		
		2-6	2.39	2.49		
		3-5	3.29	3.05		
		3-6	2.67	2.72		
		3-9	2.40	2.64		
		4-5	2.37	2.56		
		4-7	2.39	2.49		
		5-6	3.06	2.72		
		5-8	2.47	2.64		

TABLE II. (*Continued*).

N	Structure	Bond	Orthogonal 1 (Å)	Orthogonal 2 (Å)	Nonorthogonal (Å)	*Ab initio* (Å)
		6-7	3.10	2.56		
		6-8	2.95	2.68		
		7-9	2.48	2.53		
		7-10	3.79	3.77		
		7-11	2.57	2.71		
		7-12	2.38	2.48		
		8-11	3.83	3.91		
		8-13	2.39	2.51		
		9-10	2.46	2.53		
		10-11	2.50	2.68		
		12-14	2.44	2.54		
15	C_{3v}	1-2	2.77	2.66		
		1-4	2.38	2.49		
		1-5	2.79	2.59		
		1-10	2.36	2.47		
		2-3	2.45	2.56		
		2-8	2.48	2.62		
		5-14	3.14	3.14		
		11-12	2.33	2.50		
		11-14	2.60	2.59		
		13-15	2.32	2.48		
16	C_{2h}	1-2	2.44	2.59		
		1-3	2.44	2.59		
		1-5	2.50	2.59		
		1-9	2.60	2.90		
		2-3	2.40	2.55		
		3-9	2.45	2.51		
		7-11	2.52	3.25		
		8-9	2.61	2.56		
		8-10	2.97	3.54		
		8-12	2.38	2.46		
		8-15	3.27	3.17		
		9-10	2.61	2.45		
		9-14	2.33	2.46		
		10-16	3.14	2.90		
		11-13	2.36	2.52		
		15-16	3.10	2.59		
17	C_{3v}	1-2	2.39	2.52		
		1-4	3.12	2.93		
		1-8	2.43	2.55		
		1-16	2.36	2.55		
		2-4	2.38	2.53		
		2-6	2.47	2.53		
		4-6	2.46	2.55		
		4-7	3.70	3.70		
		7-9	2.48	2.51		
		7-11	2.33	2.42		
		7-14	3.49	3.52		

TABLE II. (*Continued*).

N	Structure	Bond	Orthogonal 1 (Å)	Orthogonal 2 (Å)	Nonorthogonal (Å)	*Ab initio* (Å)
		10-13	2.37	2.48		
		10-17	3.67	3.93		
		13-15	2.87	2.79		
		15-17	2.40	2.51		
18	C_{3v}	1-4	2.46	2.57		
		1-7	2.39	2.48		
		2-5	2.44	2.57		
		2-8	2.39	2.49		
		4-7	2.57	2.66		
		6-9	2.54	2.65		
		7-9	2.63	2.57		
		7-10	2.41	2.57		
		9-10	3.50	3.56		
		10-13	2.95	2.75		
		10-16	2.92	2.75		
		10-17	2.32	2.43		
		11-12	2.45	2.46		
		13-14	2.68	2.68		
		13-15	2.34	2.53		

metry. While the model of Lenosky *et al.* agreed with this structure, that for Kwon *et al.* had a distorted shape. On the other hand, the cohesive energies in these two models are similar. The cohesive energies calculated in CP-LDA and FP-LMTO methods are 4.197 and 4.70 eV, respectively, which are higher than calculated in our orthogonal models. As mentioned previously, the cohesive energy in the density functional theory without GGA correction always give lower bond lengths and higher cohesive energy. However, the bond lengths calculated by us are in reasonable agreement with the FP-LMTO method.

For Si_{10} the calculated minimum energy structure is found to be a tetracapped trigonal prismatic (C_{3v}). The cohesive energy calculated in the model of Lenosky *et al.* was very small compared to other methods, while the model of Kwon *et al.* found cohesive energy in good agreement with the nonorthogonal[28] and *ab initio* Hartree-Fock[8] methods. The bond lengths in the orthogonal tight-binding schemes are in good agreement with those obtained in the nonorthogonal tight-binding schemes and the *ab initio* results.

The calculated geometries for Si_N clusters ($N=11-18$) in the orthogonal tight-binding methods agree with those given by Ho *et al.*[18] obtained using CP-LDA theory. The main feature of these clusters is that they are built on a structural motif consisting of tricapped trigonal prism Si_9 subunits. The mobilities calculated for these prolate structures agree very well with the experiment.[18] The equilibrium structure for the Si_{19} cluster is predicted to show a transition from a prolate structure to a cagelike structure in the CP-LDA calculation.[18] On the other hand, the mobility data for this cluster support the prolate structure.[18] The equilibrium geometry of the Si_{19} cluster in the model of Lenosky *et al.* also favored a cagelike structure, whereas the model of Kwon *et al.* supported a prolate structure. This clearly suggests that the model of Lenosky *et al.* is a better method for cluster studies than the model of Kwon *et al.* Although the contradiction of theory with experiment a concerning the transition of the prolate structure from prolate to cagelike structure is not clear from the present calculations, several possibilities can be drawn from physical backgrounds. The entropic effect, which is the high temperature required to induce isomerization, does not allow the smaller cluster to become spherical in nature.[18] There could be another prolate structure which has a lower cohesive energy than the present cagelike structure. The electron correlation has an important effect on the overall stability of silicon cluster isomers.[54] In order to circumvent problems in density, functional methods, Mitas *et al.*[54] took the quantum Monte Carlo method to predict the true energy ordering. However, quantum Monte Carlo calculations show that the probability of the formation of a cagelike structure in the experiment is very small. Mobility measurements suggest that a structural transition from a prolate structure to a cagelike structure occurs at $N=24$.

The fragmentation energy, which is the energy required in removing one Si atom from a Si cluster with N atoms, was measured in fragmentation spectra.[55–57] These experiments showed that clusters with six, seven, and ten atoms should be most stable. The fragmentation energy is defined as

$$\Delta E(N)=E(N-1)-E(N). \tag{23}$$

In Fig. 5 our results are compared with the previously calculated *ab initio* results based on the LCAO-LSDA and CP-LDA schemes. Our results, based on the model of Lenosky

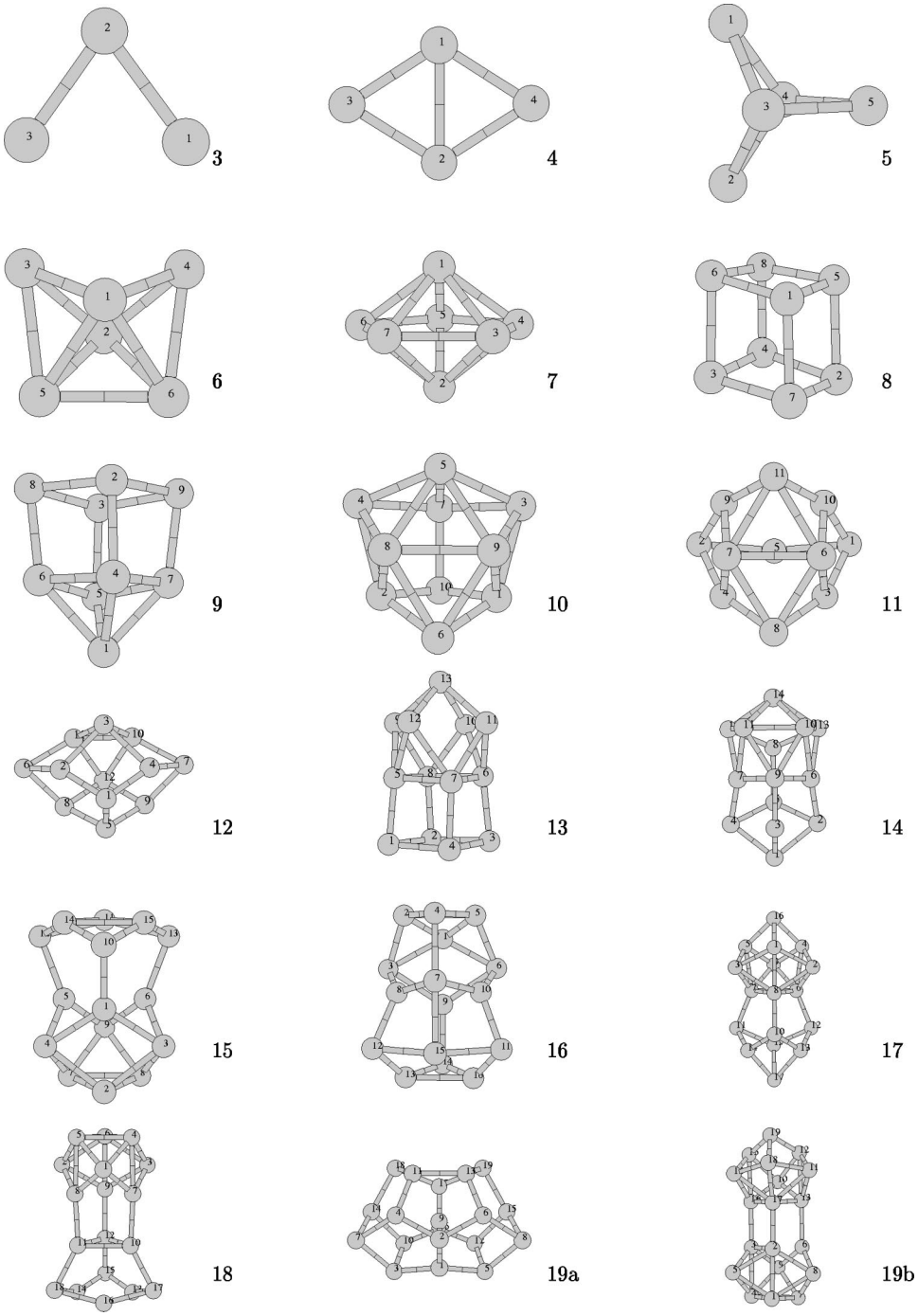

FIG. 4. Lowest-energy structures of small silicon atom clusters calculated using the orthogonal tight binding models of Ref. 38. The structures of the clusters for the model of Ref. 36 are similar, but have different bond lengths given in Table II. The atoms are numbered as in Table II.

et al., is in good agreement with the LCAO-LSDA calculations. The model of Kwon *et al.*,[36] the CP-LDA model,[18] and the nonorthogonal tight-binding model[30] predict high magnitudes. The results of all calculations show that the cluster with four, six, and ten atoms are most stable. The orthogonal models of Lenosky *et al.* and Kwon *et al.* predicted Si_{13} to be a stable cluster, whereas a CP-LDA calculation shows that the Si_{15} cluster is more stable compared to Si_{13}. Orthogonal models as well as the CP-LDA calculation show Si_{17} to be stable against fragmentation. At present we do not understand these differences.

In order to find general rules concerning the stability and equilibrium structures of small silicon clusters, we have investigated the nature of the gap energy between the highest occupied molecular orbital (HOMO) and lowest unoccupied molecular orbital (LUMO). The results are presented in Fig. 6. We have compared results obtained from the models of Lenosky *et al.* and Kwon *et al.* with the *ab initio* results given by LCAO-LSDA and CP-LDA methods. For two-atom clusters the orthogonal tight-binding scheme predicts no gap energy, while the LCAO-LSDA method predicts a high gap energy. Both empirical and density-functional-based tight-binding schemes of Tománek and Schlüter also predicted a zero gap energy for the dimer. The gap energies of the clusters obtained in the model of Lenosky *et al.* are found to be small to other methods. Recently Müller *et al.*[58] extracted

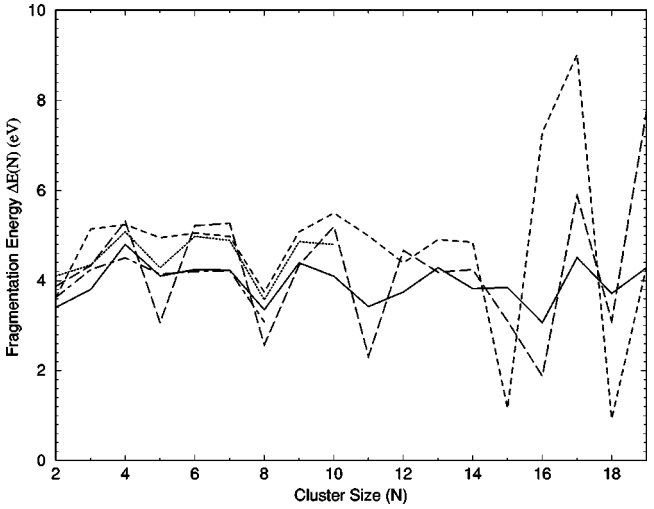

FIG. 5. Fragmentation energy in the methods of calculations of the orthogonal tight binding scheme of Ref. 38 (solid line), the orthogonal tight-binding scheme of Ref. 36 (long dashed line), the CP-LDA (Refs. 18 and 17) (dashed line) method, the nonorthogonal method of Ref. 30 (dotted line) and the gradient corrected LCAO-LSDA (Ref. 9) (dot-dashed line) method for small silicon clusters. The cagelike structure of the Si_{19} cluster is not considered here.

gap energies from the photoelectron spectra, and found that the average value is around 1.5 eV and shows a slow rise with cluster size. Clearly this gap energy is greater than the band gap in Si. On the other hand, a very recent experiment on Si clusters[59] showed that the gap energies are smaller than the band gap. In view of this experiment we find that the gap

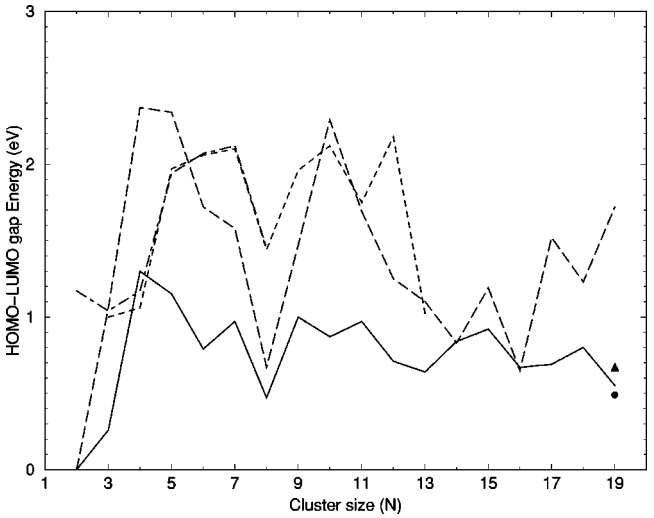

FIG. 6. Gap energy between the highest occupied molecular orbital (HOMO) and lowest unoccupied molecular orbital (LUMO) in the methods of calculation of the orthogonal tight-binding scheme of Ref. 38 (solid line), the orthogonal tight-binding scheme of Ref. 36 (long dashed line), the CP-LDA scheme (Refs. 18 and 17) (dashed line), and the gradient-corrected LCAO-LSDA method (Ref. 9) (dot-dashed line) for small silicon clusters. The filled circle and triangle are the gap energies of the cagelike structure of the Si_{19} cluster in the models of Refs. 38 and 36, respectively.

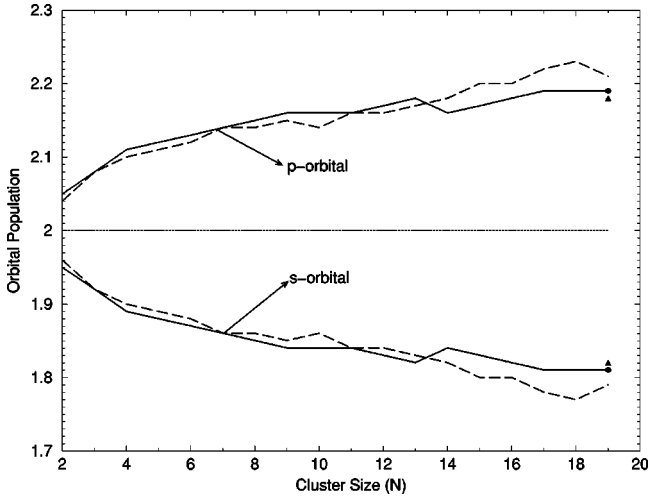

FIG. 7. Mulliken population analysis of the *s* and *p* electron levels in silicon clusters. The solid and dashed lines correspond to the orthogonal tight-binding schemes of Refs. 38 and 36, respectively. The filled circles and triangles correspond to the cagelike structure of Si_{19} in the models of Refs. 38 and 36.

energies in the model of Lenosky *et al.* are closer to the experiment than other methods of calculations.

Recently Bernstein *et al.*[60] showed that a minimal sp^3 representation is not sufficient in reproducing the conduction bands and band gap in crystalline Si. In order to reproduce the conduction bands and band gap, it is required to include *d* orbitals in the sp^3d^5 representaion. In view of this, the orthogonal tight-binding model of Lenosky *et al.* needs further improvement to calculate conduction bands accurately using a sp^3d^5 basis.

For obtaining the electronic configuration in different clusters, we carried out the Mulliken population analysis shown in Fig. 7. The results show that the configuration up to $N=19$ is nearly s^2p^2, although the model of Kwon *et al.* for $N=18$ predicted a slightly higher *p* population. The analysis of Fournier *et al.*[9] also showed that the electronic structure of Si clusters up to $N=8$ is very close to s^2p^2 for the clusters. Therefore, the clusters appear to have somewhat different bondings compared to tetrahedral bonding with sp^3 hybridization. From Fig. 4 we see that the bond angles are close to 60°, and are metallic in nature due to high coordination numbers, while in the semiconductor limit the bond angles are concentrated near 110°. The small gap energy corresponds to the metallic nature of the cluster, while the large band gap is due to the semiconductor nature. Further, the gap energy in metals normally decreases with increasing cluster size due to the electronic level quantization in a cavity. From the calculated data of Figs. 6 and 7, it appears that clusters, with the exception of dimers, are mixed metallic and semiconductor in nature. It is plausible that surface atoms tend to reduce the number of dangling bonds by taking close-packed structures. From Fig. 4 we find that clusters with $N=6-12$ take octahedral structures, with sides decorated by caps in order to stabilize the basic octahedral structure. The prolate structure for Si_N clusters ($N=13-18$) has relatively small gap energies. As expected the compact cagelike structure for Si_{19} in

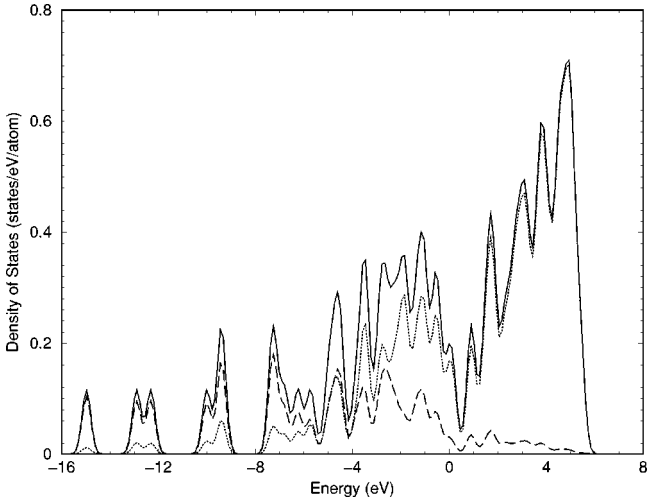

FIG. 8. Density of states for the Si_{19} cluster in the cage structure [Fig. 4(19a)]. The dashed line, dotted line, and solid line correspond to the *s* electron, the *p* electron, and the total density of states.

the models of Lenosky *et al.* and Kwon *et al.* has a lower gap energy than its corresponding prolate structure. Kaxiras estimated that the critical size of the cluster is $N=33$ for the transition of metallic to low coordination covalent bonding.[61]

The partial density of states for *s* electrons, *p* electrons, and total electrons for the cagelike structure of Si_{19} cluster is shown in Fig. 8. We find that the lower-energy levels are dominated by the *s* electrons, whereas the upper levels are decided by *p* electrons. This is also observed in bulk semiconductors, where the first and second bands are *s* like while the sp^3 hybridization is governed by the third and fourth bands.[62] The density of states for the Si_{19} cluster in the prolate structure is shown in Fig. 9. Compared to the cagelike structure there are fewer features in this structure due to less closely spaced energy levels because of the prolate structure. As expected, the density of states in both these structures do not compare with that of the bulk.

The calculated dipole moments are shown in Table III.

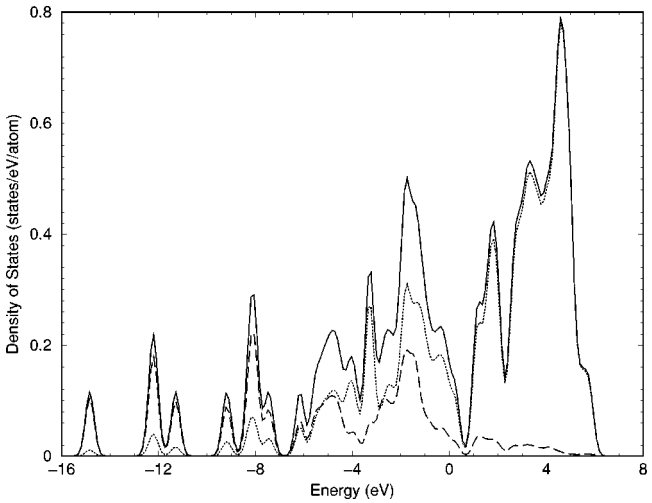

FIG. 9. Density of states for the Si_{19} cluster in the prolate structure [Fig. 4(19b)]. The notations are the same as in Fig. 8.

TABLE III. Calculated dipole moments for Si clusters in the orthogonal tight binding and pseudopotential (Ref. 15) methods. The orthogonal tight binding method of Refs. 38 (Orthogonal1) and 36 (Orthogonal2) are reported.

N	Orthogonal1 $\lvert\mathbf{p}\rvert$ (debye)	Orthogonal2 $\lvert\mathbf{p}\rvert$ (debye)	*Ab initio* $\lvert\mathbf{p}\rvert$ (debye)
2	0	0	0
3	0.42	0.41	0.33
4	0	0	0
5	0	0	0
6	0.26	0.26	0.19
7	0	0	0
8	0	0	0
9	1.26	1.26	0.36
10	1.00	0.67	0.69
11	0.55	0.55	
12	0	0	
13	0.24	0.24	
14	0	0	
15	2.86	2.86	
16	0	0	
17	1.48	1.48	
18	2.35	2.35	
19a	1.60	1.60	
19b	2.03	2.04	

The dipole moments calculated in both the orthogonal tight binding methods by Lenosky *et al.* and Kwon *et al.* are identical except for Si_{10}. The orthogonal methods are expected to show some difference from the *ab initio* method in predicting the dipole moments because of the lack of boundary conditions on the atomic wave functions in a cluster environment. Nevertheless we find that our dipole moments for Si clusters up to $N=10$ are similar to those predicted by the *ab initio* pseudopotential method, where the electron wave functions are calculated accurately.

The static polarizabilities of Si clusters calculated in the orthogonal methods of Lenosky *et al.* and Kwon *et al.* are compared in Fig. 10 with those calculated in the *ab initio* pseudopotential method by Vasiliev *et al.*[15] The polarizabilities calculated in the diagonal ansatz [Eqs. (21) and (22)] are found to be smaller than those calculated in the pseudopotential method.[15,63] With the assumption that the HOMO and LUMO provide the major contribution to the polarizability, the polarizability is inversely related to the LUMO-HOMO energy gap. Since the gap energies were higher in the model of Kwon *et al.* than in the model of Lenosky *et al.*, the calculated polarizabilities in the model of Lenosky *et al.* were higher than those in the model of Kwon *et al.* Nevertheless both orthogonal tight-binding methods predicted similar trends in polarizabilities. As discussed earlier, the expererimental gap energies are very small compared to the orthogonal tight-binding model, as a result of which the experimental polarizabilities are higher. The polarizabilities evaluated taking the atomic wave functions are found to be higher than

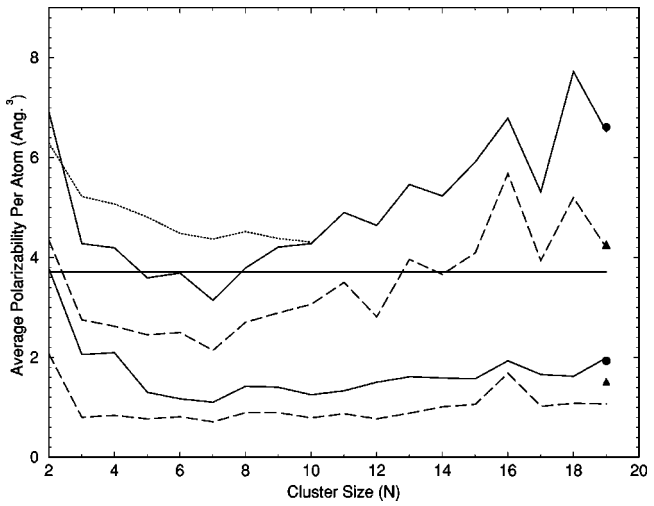

FIG. 10. Polarizabilities for Si clusters up to $N=19$ in the models of Refs. 38 (solid line) and 36 (dashed line). The polarizabilities shown above and below are calculated using atomic wave functions [Eq. (19)] and a *diagonal ansatz* [Eq. (21)], respectively. The dotted line corresponds to the pseudopotential method up to $N=10$. The polarizabilities for Si_{19} in the cagelike structure in the models of Refs. 38 and 36 are denoted by the filled circle and the triangle, respectively. The polarizability of the crystalline Si (3.71 $Å^3$) is shown by a horizontal line.

those evaluated in the diagonal ansatz, as shown in Fig. 10. Since our calculation includes the position vectors of the atoms in the wave functions, the calculated polarizabilities are smaller than those estimated by Rantala *et al.*[42]

The experimental data of Schäfer *et al.*[41] show that the polarizabilities in general should stay below the bulk limit and oscillate for cluster sizes. Our calculation shows that the polarizability increases with cluster size and stays somewhat above the bulk limit.

Finally we calculate the vibrational frequency of the dimer to test the accuracy of our calculations against other calculations and experiment. This is further necessitated since doubts were raised about the capacity of the orthogonal tight-binding method in predicting the vibrational frequencies of clusters.[27] Our calculations, using the models of Lenosky *et al.* and Kwon *et al.*, give the values of these frequencies as 414 and 523 cm^{-1}, respectively. The experimental vibrational frequency[50] is 517 cm^{-1}. Our calculations agree well with the gradient-corrected LCAO-LSDA (Ref. 9) and nonorthogonal tight-binding methods,[30] which give the values as 480 and 422 cm^{-1}, respectively. The experimental transverse optic-phonon frequency at Γ point in bulk Si is 517 cm^{-1}, which is the same as the dimer frequency. While comparing frequencies from different theoretical models with the experiment for the bulk Si, we find that the models of Lenosky *et al.*, Kwon *et al.*, and Menon and Subbaswamy estimated the frequences as 519, 716, and 586 cm^{-1}, respectively, for the bulk. The higher frequency in the model of Kwon *et al.* arises due to the steep slope of the potential at the equilibrium diamond bond length, which is a measure of the bond stretching force constant. In the case of a dimer the force constant in the model of Kwon *et al.* is higher than that of Lenosky *et al.* This shows that the prediction of Menon and Subbaswamy[29,30] about the inability of the orthogonal tight-binding scheme, in estimating the vibrational frequency, is not correct.

IV. CONCLUSIONS

In the present work we have compared two different orthogonal tight-binding schemes for optimization of structure and properties of small Si clusters. The model with a short-range radial form of the matrix elements and repulsive potential, presented by Kwon *et al.* overestimated, the cohesive energies and bond lengths. On the other hand, the method of Lenosky *et al.*, where the matrix elements and repulsive potential were calculated taking a radial cutoff up to fourth-neighbor distance in the diamond structure, correctly described cohesive energies and bond lengths. This was also supported by a nonorthogonal tight-binding scheme where a cutoff of 5.5 Å was found to bring about a good convergence in results.[30] While we establish that the orthogonal tight-binding method needs a large cutoff distance to estimate cohesive energies and bond lengths accurately it is known that the nonorthogonal tight-binding scheme does not need any such short cutoff distance.[29,30] It is further evident from the investigation that yet another drawback of the orthogonal scheme in its present form is that it predicts a lower HOMO-LUMO gap for small Si clusters, which raises doubts about the suitability of the method for describing excited states. In the future it is required that one further optimize the parameters of the tight-binding model to include excited states in order to determine the gap energies accurately.

ACKNOWLEDGMENTS

One of us (B.K.P.), acknowledges the financial support of the Indo-French cluster project No. 1508-4 to carry out this work.

[1] E.C. Honea, A. Ogura, C.A. Murray, K. Raghavachari, W.O. Sprenger, M.F. Jarrold, and W.L. Brown, Nature (London) **366**, 42 (1993).
[2] E.C. Honea, A. Ogura, D.R. Peale, C. Felix, C.A. Murray, K. Raghavachari, W.O. Sprenger, M.F. Jarrold, and W.L. Brown, J. Chem. Phys. **110**, 12 161 (1999).
[3] M.J. Jarrold and V.A. Constant, Phys. Rev. Lett. **67**, 2994 (1991).
[4] M.J. Jarrold, J. Phys. Chem. **99**, 11 (1995).
[5] K. Raghavachari and V. Logovinsky, Phys. Rev. Lett. **55**, 2853 (1985).
[6] K. Raghavachari, J. Chem. Phys. **83**, 3520 (1985).
[7] K. Raghavachari, J. Chem. Phys. **84**, 5672 (1986).
[8] K. Raghavachari and C.M. Rohlfing, J. Chem. Phys. **89**, 2219 (1988).
[9] R. Fournier, S.B. Sinnott, and A.D. DePristo, J. Chem. Phys. **97**, 4149 (1992).

[10] J.P. Perdew and Y. Wang, Phys. Rev. B **33**, 8800 (1986).
[11] R. Car and M. Parrinello, Phys. Rev. Lett. **55**, 2471 (1985).
[12] R. Car, M. Parrinello, and W. Andreoni, in *Microclusters*, edited by S. Sugano, Y. Nishina, and S. Ohnisi (Springer, Berlin, 1987), pp. 134–41.
[13] P. Ballone, W. Andreoni, R. Car, and M. Parrinello, Phys. Rev. Lett. **60**, 271 (1988).
[14] M.V. Ramakrishna and A. Bahel, J. Chem. Phys. **104**, 9833 (1996).
[15] I. Vasiliev, S. Öğüt, and J.R. Chelikowsky, Phys. Rev. Lett. **78**, 4805 (1997).
[16] S. Mukherjee, in *Trends in Atomic and Molecular Physics*, edited by K. K. Sud and U. N. Upadhyaya (Kluwer, New York, 2000), pp. 35–57.
[17] K.M. Ho, A.A. Shvartsburg, B. Pan, Z.Y. Lu, C.Z. Wang, G.W. Wacker, J.L. Fye, and M.F. Jarrold, Nature (London) **392**, 582 (1998).
[18] Z.Y. Lu, C.Z. Wang, and K.M. Ho, Phys. Rev. B **61**, 2329 (2000).
[19] U.A. Salian, S.N. Behera, and V.S. Ramamurthy, J. Chem. Phys. **105**, 3679 (1996).
[20] F. Ercolessi (unpublished).
[21] R. Biswas and D.R. Hamann, Phys. Rev. B **36**, 6434 (1987).
[22] X.G. Gong, Q.Q. Zheng, and Y.Z. He, J. Phys.: Condens. Matter **7**, 577 (1995).
[23] W.A. Harrison, *Electronic Structure and the Properties of Solids* (Freeman San Franscisco, 1980).
[24] J.C. Slater and G.F. Koster, Phys. Rev. **94**, 1498 (1954).
[25] D. Tománek and M.A. Schlüter, Phys. Rev. B **36**, 1208 (1987).
[26] K. Laasonen and R.M. Nieminen, J. Phys. C **2**, 1509 (1990).
[27] M. Menon and K.R. Subbaswamy, Phys. Rev. B **47**, 12 754 (1993).
[28] P. Ordejón, D. Lebedenko, and M. Menon, Phys. Rev. B **50**, 5645 (1994).
[29] M. Menon and K. Subbaswamy, Phys. Rev. B **50**, 11 577 (1994).
[30] M. Menon and K. Subbaswamy, Phys. Rev. B **55**, 9231 (1997).
[31] D.J. Chadi, Phys. Rev. B **29**, 785 (1984).
[32] J.L. Mercer and M.Y. Chou, Phys. Rev. B **47**, 9366 (1993).
[33] L. Goodwin, A.J. Skinner, and D.G. Pettifor, Europhys. Lett. **9**, 701 (1989).
[34] S. Sawada, Vacuum **41**, 612 (1990).
[35] M. Kohyama, J. Phys.: Condens. Matter **3**, 2193 (1991).
[36] I. Kwon, R. Biswas, C.Z. Wang, K.M. Ho, and C.M. Soukoulis, Phys. Rev. B **49**, 7242 (1994).
[37] M.S. Daw and M.I. Baskes, Phys. Rev. Lett. **50**, 1285 (1983).
[38] T.J. Lenosky, J.D. Kress, I. Kwon, A.F. Voter, B. Edwards, D.F. Richards, S. Yang, and J.B. Adams, Phys. Rev. B **55**, 1528 (1997).
[39] F. Ercolessi and J.B. Adam, Europhys. Lett. **26**, 583 (1994).
[40] Y. Luo, J. Zhao, and G. Wang, Phys. Rev. B **60**, 10 703 (1999).
[41] R. Schäfer, S. Schlecht, J. Woenckhaus, and J.A. Becker, Phys. Rev. Lett. **76**, 471 (1996).
[42] T.T. Rantala, M.I. Stockman, D.A. Jelski, and T.F. George, J. Chem. Phys. **93**, 7427 (1990).
[43] W.C. Swope, H.C. Anderson, P.H. Berens, and K.R. Wilson, J. Chem. Phys. **76**, 637 (1982).
[44] S. Kirkpatrick, C.D. Gellatt, and M.P. Vecchi, Science **20**, 671 (1983).
[45] R. Biswas and D.R. Hamann, Phys. Rev. B **34**, 895 (1986).
[46] K.D. Bonin and V.V. Kresin, *Electric-Dipole Polarizabilities of Atoms, Molecules and Clusters* (World Scientific, Singapore, 1997).
[47] Y. Wang, G.F. Bertsch, and D. Tománek, Z. Phys. D: At., Mol. Clusters **25**, 181 (1993).
[48] L. Colombo, Comput. Mater. Sci. **12**, 278 (1998).
[49] S. Hobday, R. Smith, and J. BelBruno, Nucl. Instrum. Methods Phys. Res. B **153**, 247 (1999).
[50] K.P. Huber and G. Herzberg, *Molecular Spectra and Molecular Structure, Constants of Diatomic Molecules* (Van Nostrand-Reinhold, New York, 1979), Vol. 4.
[51] C. Chatillon, M. Allibert, and A. Pattoet, C. R. Seances Acad. Sci., Ser. C **280**, 1505 (1975).
[52] G. Nilsson and G. Nelin, Phys. Rev. B **6**, 3777 (1972).
[53] B. Li, M. Qiu, and P. Cao, Phys. Lett. A **256**, 386 (1999).
[54] L. Mitas, J.C. Grossman, I. Stich, and J. Tobik, Phys. Rev. Lett. **84**, 1479 (2000).
[55] L.A. Bloomfield, R.R. Freeman, and W.L. Brown, Phys. Rev. Lett. **54**, 2246 (1985).
[56] Q.-L. Zhang, Y. Liu, R.F. Curl, F.K. Tittel, and R.E. Smalley, J. Chem. Phys. **88**, 1671 (1988).
[57] A.A. Shvartsburg, M.F. Jarrold, B. Liu, Z.-Y. Lu, C.-Z. Wang, and K.M. Ho, Phys. Rev. Lett. **81**, 4616 (1998).
[58] J. Müller, B. Liu, A.A. Shvartsburg, S. Ogut, J.R. Chelikowsky, K.W.M. Siu, K.M. Ho, and G. Gantefor, Phys. Rev. Lett. **85**, 1666 (2000).
[59] M. Marsen, M. Lonfat, P. Scheier, and K. Sattler, Phys. Rev. B **62**, 6892 (2000).
[60] N. Bernstein, M.J. Mehl, D.A. Papaconstantopoulos, N.I. Papanicolaou, M.Z. Bazant, and E. Kaxiras, Phys. Rev. B **62**, 4477 (2000).
[61] E. Kaxiras, Phys. Rev. Lett. **64**, 551 (1990).
[62] M.L. Cohen and J.R. Chelikowsky, *Electronic Structure and Optical Properties of Semiconductors* (Springer Series in Solid State Sciences: Vol. 75, Springer, New York, 1988).
[63] A. Rubio, J.A. Alonso, X. Blaze, L.C. Balbas, and S.G. Louie, Phys. Rev. Lett. **77**, 247 (1996).